JOURNAL OF PLANKTON RESEARCH | VOLUME 34 | NUMBER 9 | PAGES 802–814 | 2012

Microbial distribution and activity across a water mass frontal zone in the California Current Ecosystem

TY J. SAMO*, BYRON E. PEDLER, GREGORY I. BALL, ALEXIS L. PASULKA, ANDREW G. TAYLOR, LIHINI I. ALUWIHARE, FAROOQ AZAM, RALF GOERICKE AND MICHAEL R. LANDRY

SCRIPPS INSTITUTION OF OCEANOGRAPHY, UNIVERSITY OF CALIFORNIA, SAN DIEGO, LA JOLLA, CA 92093-0202, USA

*CORRESPONDING AUTHOR: tsamo@ucsd.edu

Received November 4, 2011; accepted in principle May 24, 2012; accepted for publication June 2, 2012

Corresponding editor: John Dolan

Ocean fronts with accumulated biomass and organic matter may be significant sites of enhanced microbial activity. We sampled a frontal region (the A-Front) separating oligotrophic and mesotrophic water masses within the California Current Ecosystem (CCE) to assess the influence of frontal hydrography on several microbial parameters. Samples for heterotrophic bacterial, viral and flagellate abundance, dissolved and particulate carbon and nitrogen, transparent particles and bacterial carbon production were collected at 6 depths from the surface to 100 m with 5–9 conductivity/temperature/depth casts along a 26-km northerly transect across the front. Relative to adjacent oligotrophic and mesotrophic waters, the frontal transition displayed peaks in the mean estimates of cell-specific bacterial carbon and bulk bacterial production, particulate organic carbon and particulate organic nitrogen concentrations, and the abundance and size of transparent particles. Bacterial carbon production increased ~5-fold northward from oligotrophic waters to the frontal zone, in agreement with an increase in the frequency of dividing cells, but bacterial abundance was lower than at adjacent stations. This may be partially explained by high chlorophyll, elevated virus:bacteria ratios and low nanoflagellate grazer abundance at the front. Our data suggest that CCE fronts can facilitate intense biological transformation and physical transport of organic matter, in sharp contrast to adjacent low productivity waters, and harbor dynamic microbial populations that influence nutrient cycling.

KEYWORDS: bacteria flagellates; viruses; organic matter biogeochemistry; A-Front California Current

INTRODUCTION

The California Current Ecosystem (CCE) is a seasonally dynamic region that contains oligotrophic offshore and highly productive coastal environments. Eastern boundary currents and wind-driven upwelling events combine with the current divergence near Point Conception, California, creating distinct water masses that extend southward (Bray *et al.*, 1999; Rykaczewski and Checkley, 2008). As these cold, mesotrophic water parcels contact warmer oligotrophic waters offshore of the Southern California Bight, frontal zones with sharp gradients and filaments of sea surface temperature (SST) and chlorophyll often form at the junction, exhibiting variable spatiotemporal frequencies controlled by

doi:10.1093/plankt/fbs048, available online at www.plankt.oxfordjournals.org. Advance Access publication June 29, 2012

local forcings and temperature gradients (Kahru *et al.*, 2012).

Driven by primary and secondary circulation from geostrophic and ageostrophic processes (Franks, 1992; Claustre *et al.*, 1994), the confluence of water masses at fronts can result in fertilization and horizontal advection. This can lead to the growth and accumulation of plankton at fronts or within frontal jets. Responses of microbial communities can vary, underscoring the importance of physical features in biological processes. Studies in the southwestern Mediterranean Sea examined the effects of the Almeria-Oran geostrophic front in the eastern Alboran Sea (Prieur and Sournia, 1994). Frontal zones were characterized by elevated primary production rates and diatom-dominated communities (Fiala *et al.*, 1994), enhanced bacterial carbon production (BCP) (Fernández *et al.*, 1994) and increases in particle export (Peinert and Miquel, 1994). In the subtropical convergence zone of the Sargasso Sea, enhanced nutrient fluxes across the transition zone led to increased chlorophyll *a* (chl *a*), though without a concomitant heterotrophic bacterial response (Riemann *et al.*, 2011). Mesoscale blooms of phytoplankton have also been attributed to upwelling at fronts in the northern CCE (Pallàs-Sanz *et al.*, 2010). Others have examined the influence of cyclonic and anticyclonic eddies on primary and secondary production (Ducklow and Hill, 1985; Falkowski *et al.*, 1991; Ewart *et al.*, 2008). Consistently, the injection of inorganic nutrients stimulated phytoplankton growth, resulting in biomass and organic matter accumulation relative to adjacent waters.

Dissolved organic matter (DOM) produced by phytoplankton and other microorganisms is important in marine biogeochemical cycles and climate regulation (Aluwihare and Repeta, 1999; Raven and Falkowski, 1999; Azam and Malfatti, 2007). The biogeochemical fate of DOM is largely regulated by the heterotrophic activity of marine prokaryotes (bacteria and archaea, here collectively called "bacteria") (Hagström *et al.*, 1984). The efficiency with which bacteria utilize the DOM of varied quality to create new biomass or, alternatively, respire carbon, ultimately determines the relative partitioning of carbon into labile, semi-labile and refractory organic matter classes, influencing global ocean–atmosphere carbon dioxide (CO_2) exchange and carbon export (del Giorgio and Cole, 1998). These processes influence carbon export via the biological pump operating through the microbial loop (Azam *et al.*, 1983; Martin *et al.*, 1994; Karl *et al.*, 1998).

Studies on the roles of microbes in carbon cycling at oceanic fronts have shed light on the role of hydrography in regulating the metabolism and growth of photoautotrophic and heterotrophic microbes. Nutrient injections in frontal zones, as well as meso- and submesoscale instabilities, often support enhanced bacterial production due to increased primary production by larger phytoplankton (Videau *et al.*, 1994; Morán *et al.*, 2001), but the mechanisms are not clear. Alternatively, fronts can support a food web characterized by abundant picophytoplankton where elevated bacterial production may be due at least in part to the release of top-down grazer control modulated by flagellates (Heinänen *et al.*, 1995). Such variability in bottom-up versus top-down control of marine bacterial populations at frontal zones has also been observed at the Almeria-Oran front (Van Wambeke *et al.*, 2004), and the relative contributions of these two mechanisms to microbial ecological dynamics in the Mediterranean region was found to differ between oligotrophic, frontal and gyre systems. Such interactions between hydrodynamics and biological responses are likely to determine the extent to which bacteria, phytoplankton and organic matter impact local food webs as well as the CO_2 exchange with the atmosphere (Sempéré *et al.*, 2003).

The microbial influences on carbon cycling at frontal zones have not been well studied in the CCE, nor has a baseline of microbial activities or abundance within these features been established in this region. As a component of the California Current Ecosystem—Long Term Ecological Research (CCE-LTER) site, we investigated a frontal boundary, designated the A-Front, between abutting oligotrophic and mesotrophic water masses to assess patterns, gradients and implications of microbially mediated carbon cycling. The results are discussed within the comprehensive ecosystem context of this CCE-LTER study.

METHOD

We sampled a 26-km transect of nine stations across a deep water front (Landry, Ohman *et al.*, 2012; Ohman *et al.*, 2012) located 350 km west of San Diego in the southern CCE (Fig. 1). All samples were collected during 24–25 October 2008 over a 9 h period at night (21:30–05:00, local time) with Niskin bottles on a conductivity/temperature/depth (CTD) rosette. Based on satellite images of the SST and chl *a*, hydrography, nutrients and biological parameters, stations 1–3 were located on the oligotrophic side of the front, stations 4 and 5 were designated frontal and stations 6–9 were on the mesotrophic side. Unless otherwise noted, microbial variables were measured from 0 to 100 m depths at stations 1, 3, 5, 7 and 9. Data for temperature, salinity and density were

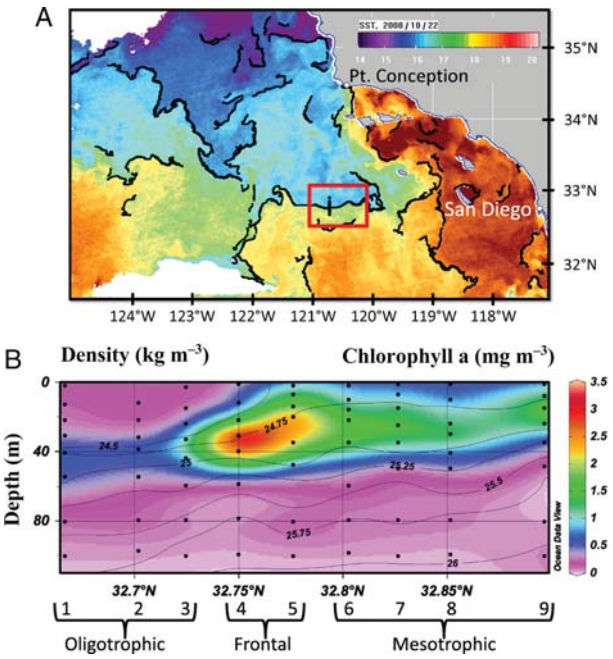

Fig. 1. Satellite images of the sea surface temperature (**A**) with the study area indicated by the red box. The section plot of chlorophyll *a* concentration across the front with density contours (**B**).

obtained from the shipboard CTD package (Sea-Bird Electronics, Inc., Bellevue, WA, USA).

Bacterial abundance, biomass and frequency of dividing cells

Water samples (3 mL) were fixed with 2% (final) formaldehyde, filtered on white 0.2-μm pore size 25-mm diameter polycarbonate filters (Nuclepore, GE Whatman, Piscataway, NJ, USA), dried at room temperature and stored at −20°C. Each filter was mounted and stained with VECTASHIELD containing 1.5 μg mL^{-1} of 4′, 6-diamidino-2-phenylindole (DAPI, Vector Laboratories, Burlingame, CA, USA), and imaged at 1000× magnification on a Nikon TE2000-U inverted epifluorescence microscope using a CoolSnapHQ CCD camera connected to NIS-Elements 3.2 software. Ten image fields per filter were processed to measure cell abundance, length and width using the signal thresholding and binary layer functions of the software. Cyanobacteria were excluded from the total bacterial counts by manual removal from the DAPI channel identified as autofluorescent cells in the TRITC channel (excitation 555 ± 14 nm, emission 617 ± 37 nm). An area cutoff of 0.1–2 μm^2 was used to exclude viral-like particles (VLP) and protists from the analyses. The average cell number per field was converted to abundance, and the dimensions of the cells were used to calculate biovolumes (μm^3 cell^{-1}) based on the equation $V = (\pi/4) \times W^2 \times (L - W/3)$ (Bratbak, 1985). Biovolumes were converted to per cell protein content (fg cell^{-1}) using the power law function $P=88.6*V^{0.59}$, and multiplied by 0.86 to calculate cell-specific carbon (fg C cell^{-1}) (Simon and Azam, 1989). DAPI-based biovolume estimates were found to be acceptable in a previous calibration study using atomic force microscopy (Malfatti *et al.*, 2010). Cell carbon values for each depth were averaged, then multiplied by the cell abundance to calculate the bacterial carbon (BC) concentration (μg C L^{-1}).

The frequency of dividing cells (FDC) was calculated according to Hagström *et al.* (Hagström *et al.*, 1979). Septated cells were counted from the same fields used for the total cell abundance and divided by the total number of bacteria from each field. The numbers were arcsine transformed to ensure normality of the data and correct averaging of percentages, and then back-transformed to obtain a percentage for each depth.

Heterotrophic bacteria were also enumerated by flow cytometry (FCM) from stations 1–9 and depths from the surface down to 80 m. Two milliliter samples were preserved (0.5% paraformaldehyde; final) and then flash frozen in liquid nitrogen. Onshore, the samples were stored at −80°C until shipment to the University of Hawaii FCM facility (SOEST Flow Cytometry Facility, www.soest.hawaii.edu/sfcf). Samples were thawed and stained with Hoechst 33342 (1 μg mL^{-1} final concentration) (Monger and Landry, 1993). A Beckman-Coulter Altra flow cytometer was mated to a Harvard Apparatus syringe pump for quantitative analyses, and equipped with two argon ion lasers tuned to UV (200 mW) and 488 nm (1 W) excitation (Coherent, Inc., Santa Clara, CA, USA). Scatter (side and forward) and fluorescence signals were collected. Fluorescence signals were normalized to 0.5 and 1.0-μm yellow–green polystyrene beads (Polysciences, Inc., Warrington, PA, USA). Data generated as listmode files (FCS 2.0 format) were acquired from the flow cytometer using Expo32 software (Beckman-Coulter). FlowJo software was used to assign population designations from the data based on scatter and fluorescence signals (Tree Star, Inc., www.flowjo.com). Autotrophic bacteria, *Prochlorococcus* and *Synechococcus*, identified, respectively, by their chl *a* and phycoerythrin autofluorescences, were excluded from FCM estimates of total (heterotrophic) bacteria.

Microscopy-based counts (MIC) from every other station were not well resolved between stations or with depths from 40 to 100 m. To compensate for unsampled stations and depths, two regression plots (intercepts set to 0) were made between MIC- and

FCM-based measurements. One showed a strong relationship in MIC versus FCM-derived cell counts (MIC = 0.850*FCM; $R^2 = 0.958$, $P < 0.0001$; Supplementary data, Fig. S1A); the other examined MIC-based carbon biomass (BC, μg C L^{-1}) versus the product of FCM-derived cell counts and FCM-derived normalized, mean DNA fluorescence (BC = 8.122 FCM*DNA; $R^2 = 0.644$, $P < 0.0001$; Supplementary data, Fig. S1B). We used the slopes of these regressions to estimate BC at stations 2, 4, 6 and 8 and for bacterial abundances at stations 1–3 and 7–9, both to a depth of 80 m. Microscope counts were used for 100 m and surface samples at the front station and mesotrophic stations due to consistent deviations in MIC–FCM regressions for those samples.

Viral abundance and virus:bacteria ratios

Viral abundance was determined for 0–80-m depths at stations 4, 5 and 6. Samples were fixed with 0.5% (final) EM-grade glutaraldehyde, flash frozen in liquid nitrogen and stored at −80°C (Brussaard, 2004). After thawing, 500 μL was filtered (≤25 cm Hg) onto 0.02-μm pore size aluminum oxide filters (Anodisc 25, GE Whatman, Piscataway, NJ, USA), stained with SYBR Gold (Invitrogen, Carlsbad, CA, USA; 0.25% final concentration of original stock) and mounted onto glass slides with anti-fade solution (0.1% *p*-phenylenediamine in phosphate-buffered saline:glycerol at 1:1 concentration). At least 200 viruses per sample were counted on an Olympus BX51 microscope at 1000× magnification using wide-field excitation centered at 470–490 nm with a long pass emission filter (Patel *et al.*, 2007). Bacterial counts were made on the same filters to calculate the virus:bacteria ratios.

Nano- and microflagellate enumeration

Heterotrophic nano- and microflagellates were counted in 50 and 500 mL samples, respectively. Samples were preserved sequentially with alkaline Lugol's solution, formalin and sodium thiosulfate, stained with proflavin and DAPI, concentrated onto 25-mm diameter 0.8- and 8-μm black polycarbonate filters (for nano- and microflagellates, respectively), and mounted on slides. Samples were digitally imaged at 630× (nano) or 200× (micro) using a Zeiss Axiovert 200 M inverted compound epifluorescence microscope. Images were processed with Image Pro software. Nano- and microheterotrophs were distinguished by the cell length (2–20 versus 20–200 μm) and lack of chloroplasts or significant red chlorophyll fluorescence. Details are described in an accompanying paper by Taylor *et al.* (Taylor *et al.*, 2012).

Chlorophyll *a* concentration

Chlorophyll *a* was measured by high-performance liquid chromatography (HPLC). Seawater volumes (2.2 or 4.4 L) were filtered onto Whatman GF/F filters, stored in liquid nitrogen, extracted in acetone and analyzed by HPLC (Goericke, 2002) and described by Taylor *et al.* (Taylor *et al.*, 2012).

Bacterial carbon production

The leucine incorporation method was used to estimate the rates of BCP. Samples (2 mL) were incubated with 20 nM of L-[4,5-^{3}H] leucine in the dark for 1 h at *in situ* temperature in triplicate with duplicate 5% TCA-killed controls (Kirchman *et al.*, 1985; Smith and Azam, 1992). Samples were then filtered on either 0.2-μm or 1-μm pore size polycarbonate filters (total or >1-μm BCP). Three successive additions of 1 mL 5% TCA were made and left without suction for 30 s. This approach was used in the response to measurements on a previous cruise and laboratory experiments that revealed anomalously wide-ranging values on filters when the sample was first fixed with formaldehyde or TCA. We assumed that negligible amounts of labeled proteins passed through the filter prior to TCA precipitation. Each filter was dried in a glass scintillation vial at room temperature. Onshore, EcoLite scintillation cocktail was added to each vial and analyzed in a Beckman LS6000A liquid scintillation counter. Conversion of leucine incorporation to estimate the carbon production rate was performed assuming 3.1 kg C mol^{-1} leucine (2× isotope dilution) and 24 h day^{-1} (Simon and Azam, 1989).

Organic and inorganic nutrients

Seawater samples (40 mL) from stations 1–9 were acidified with hydrochloric acid to pH∼2 for total organic carbon (TOC) and total nitrogen (TN) analyses on a Shimadzu 500 V-CSN/TNM-1 TOC. Quantification used seven-point C and N standard curves in conjunction with consensus reference material (RSMAS, University of Miami) interspersed between samples. The consensus reference material routinely measured values in the range 41 and 45 μM C. Filtration was not done prior to TOC determination to minimize contamination. Although particulate organic carbon (POC) values were available (below), the dissolved organic carbon (DOC) was not computed as the difference between the TOC and the POC because the determinations were made on different volumes (100 μL injections versus 2 L filtrations) and because the DOC was

typically higher than the POC by an order of magnitude. So, the TOC can be assumed to be mostly composed of the DOC. Total organic nitrogen (TON) concentrations, on the other hand, may be strongly influenced by particulate organic nitrogen (PON) as their values can be similar during phytoplankton bloom conditions.

Samples for analyses of ammonium (NH_4^+), nitrate (NO_3^-) and nitrite (NO_2^-) were taken from the same depths and Niskin bottles as those for TOC and TN. Nitrate concentrations determined during California Cooperative Oceanic Fisheries Investigations (CalCOFI) survey cruise 0810, located in the same area during 14 and 30 October 2008, were also used (below). Dissolved inorganic nitrogen (DIN; nitrate plus nitrite, in this case) must be subtracted from TN to calculate TON. In this study, TON concentrations were calculated for all depths <60 m. Below these depths DIN and TN were too similar to allow for accurate TON determination. Nitrate concentrations were available from the A-Front cruise. However, when nitrate and phosphate concentrations and ratios in water masses with similar densities were compared between A-Front and CalCOFI 0810 it was apparent that A-Front nitrate samples may have been compromised. Therefore, nitrate concentrations measured during CalCOFI 0810, in water masses with similar density and phosphate concentration characteristics to those sampled for TN during A-Front, were used to compute the TON. This assumed that phosphate concentrations did not change independently of nitrate in a particular water mass of the same density between the two cruises.

Two liters of seawater were filtered onto 25 mm precombusted (450°C, 6 h) Whatman GF/F filters for POC and PON determinations. Filters were exposed to concentrated HCl vapors to remove inorganic carbon, oven-dried overnight and one-half of each filter was analyzed for C and N at the Scripps Institution of Oceanography's Analytical Facility using a Costech Elemental Analyzer (Costech Analytical Technologies, Valencia, CA, USA) according to standard protocols.

Transparent particles

Following fixation with 2% formaldehyde (final), 20 mL seawater samples were filtered on 1-μm pore size polycarbonate membranes. With vacuum released, 500 μL of Alcian blue (0.2-μm filter-sterilized solution of 0.02% Alcian blue + 0.06% acetic acid in milli-Q water) was then added on the filter and allowed to stain for 30 s, after which vacuum was reapplied and the filter was dried at room temperature and stored at −20°C for analysis onshore (Alldredge *et al.*, 1993). In the laboratory, the filters were placed on 100 μL drops of 1× SYBR Gold, incubated for 15 min, then removed and allowed to fully dry on absorbent paper and mounted onto microscope slides using Resolve immersion oil (Richard Allan Scientific, Kalamazoo, MI, USA). Filter fluorescing particles (FFP) were counted at ×600 magnification on an Olympus BX51 epifluorescence microscope using wide field excitation centered at 470–490 nm with a long pass emission filter. Counts were made from 20 haphazardly selected fields on each slide, and the area of each particle was estimated using the ocular grid of the microscope (Samo *et al.*, 2008). Transparent exopolymer particles (TEP) were quantified on the same preparations using sub-stage illumination that was diffused through a Cytoclear slide (Sterlitech Corp, Kent, WA, USA) placed below the slide holding the mounted filter (Alldredge *et al.*, 1993; Samo *et al.*, 2008).

Contour and section plots

Data collected along the transect was heterogeneous and unevenly spaced in both the horizontal and vertical axes. The contouring and shading of the DIVA gridding algorithm in Ocean Data View was therefore used to create all section and contour plots (Schlitzer, 2008).

RESULTS

Distributions of chlorophyll *a* and bacterial abundance and biomass

The maximum chl *a* concentration among all stations and depths was found at ~30 m from the frontal station 4, coinciding with the $\sigma_\theta = 24.75$ isopycnal (3.20 μg L^{-1}). Frontal station 5 also exhibited a chlorophyll maximum of 2.46 μg L^{-1} at the $\sigma_\theta = 24.75$ isopycnal (Fig. 1B). Integrated chlorophyll was maximal at stations 4 and 5, and station 5 also exhibited the highest integrated BCP (Table I). The nitracline, defined as the depth where nitrate concentration exceeds 1 μM, was located at 42 m at the southernmost station 1 in oligotrophic waters and shoaled to 21 m at the northernmost mesotrophic station 9 (Table I). The detailed depth profile data collected at the transect stations are provided in Supplementary data, Table S1.

Bacterial abundance in the southern, oligotrophic surface waters was typically 10^9 L^{-1}, decreasing to 10^8 cells L^{-1} below 40 m (Fig. 2A). The depth profile at the front was slightly different, with lower abundance at the surface and a greater variability in abundance with depth, which ranged from ~5×10^8 to 10^9 cells L^{-1}.

Table I: Summary values of the nitracline depth and integrated stocks of chlorophyll, bacterial carbon, bacterial carbon production and calculated bacterial growth rate

Station	Latitude (°N)	Longitude (°W)	Nitracline depth (m)	Integrated chl a′	Integrated BC (mg C m^{-2})	Integrated BCP (mg C m^{-2} day^{-1})	Bacterial growth rate (day^{-1})
1	32.6667	120.7098	42	30.1	1770	153	0.0863
2	32.7018	120.7085	39	25.3	983		
3	32.7247	120.7075	31	33.9	1230	159	0.129
4	32.7498	120.7088	36	94.4	1420		
5	32.7762	120.7077	32	98.1	1520	698	0.459
6	32.8027	120.7097	28	66.3	2190		
7	32.8263	120.7097	29	56.4	2190	406	0.185
8	32.8515	120.7105	25	51.7	2560		
9	32.8965	120.7082	21	45.8	3240	301	0.0929

Depth integrated values were calculated from the surface to 100 m.

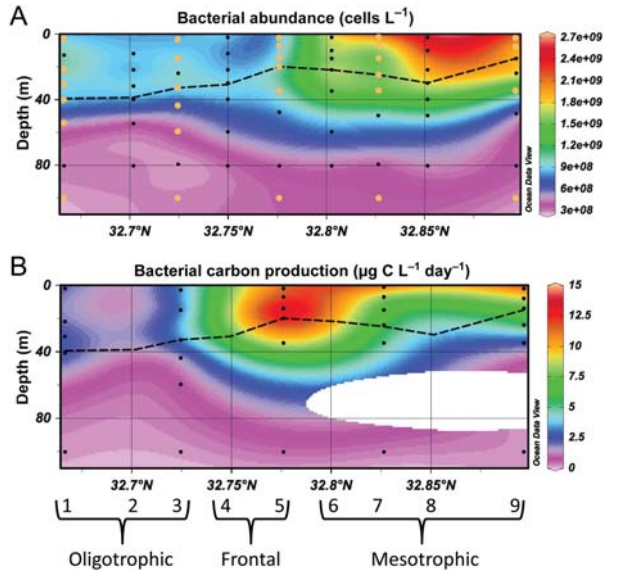

Fig. 2. Bacterial abundance (**A**) and bacterial production (**B**) along the A-Front transect. Stations are identified by numbers with water masses bracketed. Beige circles within each plot denote microscopy-based data when flow cytometry was used to augment the abundance and total carbon datasets. The dashed line denotes the depth of maximum chlorophyll concentrations.

Abundances in the northern, mesotrophic waters were substantially higher, ranging $1.50-2.25 \times 10^9$ cells L^{-1}. Comparison of the BCP and BC (Fig. 2B; Supplementary data, Fig. S2B) with chlorophyll (Fig. 1B) revealed these measurements to be effectively bounded by the depth of the chlorophyll maximum. The depth of maximum BCP at station 5 was coincident with the depth of maximum chlorophyll.

Cell-specific BC was highest at the southernmost (oligotrophic; 27 fg C $cell^{-1}$) and northernmost (mesotrophic; 28 fg C $cell^{-1}$) stations compared with adjacent stations (14–20 fg C $cell^{-1}$; Supplementary data, Fig. S2A), and a relatively high value was also found at the surface of the front (29 fg C $cell^{-1}$). Profiles of BC followed a pattern similar to cell abundance, with highest values at the northernmost station, and thus appeared to be driven by this parameter and not cell-specific carbon.

Bacterial carbon production

BCP strongly reflected the frontal boundary. Maxima of 11–13 µg C L^{-1} day^{-1} were measured from the surface to ~40 m at the front, with enhanced production shoaling to the surface on the northern, mesotrophic side (Fig. 2A). Bacterial production in southern, oligotrophic waters was low, averaging a quarter of that at the front (~3 µg C L^{-1} day^{-1}). These patterns were corroborated by nearly identical profiles of >1-µm fractionated carbon production values (data not shown) and the FDC at each depth, both of which exhibited shallow, subsurface maxima at the front (Supplementary data, Fig. S2C). Furthermore, growth rates calculated by dividing depth-integrated BCP by depth-integrated BC (e.g. Ducklow, 2000) exhibited the highest value (0.46 day^{-1}) at the front, decreasing to 0.1 day^{-1} north and south of the front (Table I).

Viral abundance and virus:bacteria ratios

Viral abundance at the surface of the front was $1.5-2 \times 10^{10}$ VLP L^{-1}, and decreased to 5×10^9 VLP L^{-1} <50 m (Supplementary data, Fig. S3A). The mesotrophic station showed a similar trend, but elevated viral abundance extended deeper than 30 m. The oligotrophic station exhibited viral abundances of $1-1.5 \times 10^{10}$ particles L^{-1} from the surface to a depth of 40 m.

Bacterial abundances at station 5 calculated from Anodisc filters using the BX51 Olympus microscope were not significantly different from those measured on

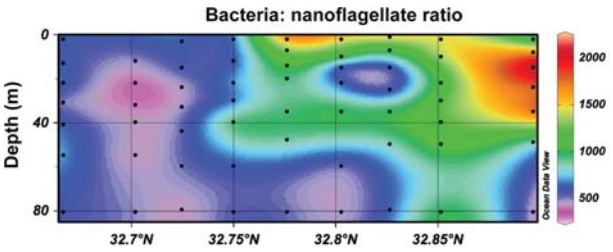

Fig. 3. Bacteria:nanoflagellate ratios across the front. In comparison with the oligotrophic and mesotrophic stations, frontal zone nanoflagellates were less abundant, thereby increasing the bacteria:nanoflagellate ratios.

polycarbonate filters using the Nikon TE2000-U microscope (Student's *t*-test, $P = 0.265$), and were therefore deemed appropriate for calculating virus:bacteria ratios. The highest virus:bacteria ratio of 23:1 was observed at the surface of the front, decreasing to 17:1 and then to 10:1 <20 m (Supplementary data, Fig. S3B).

Nano- and microflagellate abundance

Nanoflagellate abundances were evenly distributed from the surface to 40 m both south and north of the front. At the front, abundances were on the order of 4×10^5–1×10^6 L^{-1}, or ~20–50% of those at the northern and southern adjacent stations (Supplementary data, Table S1). Bacteria:nanoflagellate ratios increased along the transect, 3- to 4-fold at the surface of the station 5 frontal zone and at 15 m in the northernmost station (Fig. 3). Microflagellate abundances generally increased from south (~10^3 cells L^{-1}) to north (~8×10^3 cells L^{-1}) and showed maxima at the mesotrophic stations from the surface to 30 m (Supplementary data, Table S1). Unlike nanoflagellates, microflagellate abundance did not decrease markedly at the front, but was more evenly distributed throughout the sampled water column.

Organic and inorganic nutrients

The TOC and POC concentrations were poorly correlated, and subsequent analyses and discussion are based on the premise that the TOC reflects the distribution of the DOC. Slightly higher TOC values at the front coincided with locations of highest BCP and chl *a* (Figs 1B and 2B). Maximal mean depth-integrated concentrations occurred at station 3, with depth-specific maxima from 0 to 20 m (Table II and Supplementary data, Fig. S4A). Station 8 had the highest mean depth-integrated and depth-specific TON, with high values also present at stations 3–6 throughout the water column. Depth-specific POC and PON were elevated at the front and highest at station 2. Mean depth-integrated values did not follow this trend and displayed highest values at station 2 (POC) and 6 (PON). Overall, the profiles were similar to *chl a*, indicating that these measurements reflected depth distribution of biomass concentrations. The DIN, POC/PON and TOC/TON data (Table II and Supplementary data, Table S2) are discussed below as they pertain to microbial activity.

Transparent particles

TEP and FFP differed in concentration and size along the transect (Supplementary data, Fig. S5 and Table S2). The maximal TEP concentration centered <40 m and south of the front. Concentrations of TEP at the front were enhanced relative to northern waters while FFP concentrations were highest at the surface in the oligotrophic and northernmost stations. Average areas of each particle size class were also distributed differently with depth, but showed some agreement at the surface of the front where FFP average areas decreased from ~1000 to 200 μm^2 <20 m while maintaining high values northward into the mesotrophic waters.

DISCUSSION

We hypothesized that elevated nutrient fluxes associated with the A-Front (Li *et al.*, 2012) would elicit strong metabolic responses and enhanced primary production, and result in elevated heterotrophic activities, thus affecting carbon cycling at the meso- to submesoscale. The characteristics and responses of primary producers and heterotrophic bacteria highlighted the active and dynamic nature of this frontal zone. Depending on the magnitude of along isopycnal and frontal jet transport of these microbial communities and their biogeochemical influence on inorganic and organic nutrients, such sites may play an important role in nutrient cycling on larger spatial scales.

Bacterial responses at the front

A striking observation was the enhanced rate of depth-integrated and depth-specific BCP at the front (Table I and Fig. 2B). Maximal BCP of ~13 μg C L^{-1} day^{-1} at 15 m indicated increased bioavailability of DOM and essential nutrients. The range of BCP estimates at the A-Front was within the range of previous measurements in the Southern California Bight region of the CCE (0.28–14 μg C L^{-1} day^{-1}; Fuhrman *et al.*, 1985, assuming 20 fg C cell^{-1} and 1.18×10^{18} cells mol^{-1} TdR;

Table II: Mean depth integrated values of organic carbon, organic nitrogen and ratios along the A-Front transect

Station	Latitude (°N)	Longitude (°W)	Depth of integration (m)	Mean integrated TOC (mg m^{-2})	Mean integrated TON (mg m^{-2})	Mean integrated POC (mg m^{-2})	Mean integrated PON (mg m^{-2})	Mean integrated TOC:TON	Mean integrated POC:PON
1	32.6667	120.7098	41	7900	530	798	120	14.9	6.64
2	32.7018	120.7085	39	7430	502	1530	239	14.8	6.43
3	32.7247	120.7075	44	9160	617	975	148	14.9	6.61
4	32.7498	120.7088	40	7920	628	1360	241	12.6	5.65
5	32.7762	120.7077	35	6820	607	1050	254	11.2	4.14
6	32.8027	120.7097	35	6370	605	1210	270	10.5	4.48
7	32.8263	120.7097	35	6050	577	1290	266	10.5	4.84
8	32.8515	120.7105	40	7490	763	1120	238	9.81	4.72
9	32.8965	120.7082	35	5790	541	961	188	10.7	5.12

TOC, total organic carbon; TON, total organic nitrogen; POC, particulate organic carbon; PON, particulate organic nitrogen.

Simon *et al.*, 1990, assuming 3.1 kg C mol^{-1} Leu), and within the range of seasonally estimated rates in the Arabian Sea (0.50–15.0 μg C L^{-1} day^{-1}; Ducklow *et al.*, 2001, assuming 3.1 kg C mol^{-1} Leu). They were greater than those measured in the Santa Monica Basin (~2.0 μg C L^{-1} day^{-1}; Cho and Azam, 1988, assuming 20 fg C cell^{-1} and 1.18×10^{18} cells mol^{-1} TdR), and the North Atlantic (0.50–10.0 μg C L^{-1} day^{-1}; Hoppe *et al.*, 2002, assuming 3.1 kg C mol^{-1} Leu), yet lower than peak values in the South Atlantic Ocean (0.94–16.6 μg C L^{-1} day^{-1}; Hoppe *et al.*, 2002, assuming 3.1 kg C mol^{-1} Leu).

The enhanced depth-integrated bacterial growth rates, high FDC, high chl *a* concentration and the significant correlation between BCP and chl *a* ($R^2 = 0.622$, $P < 0.0001$) at the front suggest that this oceanographic feature supported enhanced bacterial growth. These results are in agreement with previous work noting the positive correlation between chl *a* (and/or primary production) and heterotrophic bacterial activity and growth rates in aquatic systems (Cole *et al.*, 1988). Bacteria–phytoplankton interactions are facilitated by the release of labile DOM from phytoplankton (Mague *et al.*, 1980). Heterotrophic bacteria rapidly metabolize labile organic matter (Kirchman *et al.*, 1991), causing nutrient remineralization, as we saw at station 5 (frontal) at 100 m where BCP was 1.4–2.6 times greater than either the oligotrophic and mesotrophic stations at 100 m. Thus, microbial activity within the frontal zone likely exerted substantial influence on elemental cycling within and below the euphotic zone of the CCE.

POC and PON were highest at the front (Supplementary data, Fig. S4C and D). These measurements reflected localized high phytoplankton biomass and underscored the uniqueness of the A-Front as a region within the CCE where bloom conditions were closely flanked by less productive waters. However, TOC was, in fact, lower at the A-Front relative to adjacent oligotrophic waters (Table II and Supplementary data, Fig. S4A). Thermal stratification can lead to the accumulation of semi-labile and refractory DOM with reduced influx of inorganic nutrients, which limits bacterial processing of DOC in warm, oligotrophic waters (Hansell and Waterhouse, 1997). The TOC was negatively correlated with density ($R^2 = 0.832$) in our study region. However, at the lowest densities, TOC concentrations were higher than predicted by simple physical mixing. This observation is consistent with greater accumulation of semi-labile TOC in warm surface water south of the front. Additionally, reduced DOC consumption by heterotrophic bacteria due to grazing or insufficient nutrients can result in an accumulation of DOC (Thingstad *et al.*, 1997). Enhanced carbon-rich POM at the southern stations, seen as high POC/PON signatures (>6.6: Supplementary data, Table S2) (Redfield *et al.*, 1963), suggests preferential degradation of nitrogenous organic matter in the oligotrophic system (Kähler and Koeve, 2001).

We note that the TOC/TON was in agreement with other values for the North Pacific Ocean—between 13 and 20 (Supplementary data, Table S2) (Hansell and Waterhouse, 1997; Libby and Wheeler, 1997; Ogawa and Tanoue, 2003). The marginal differences were confined to each water mass, i.e. the southern oligotrophic (stations 1–3), the front and adjacent depths (stations 4–6) and the northern mesotrophic (stations 7–9). The lower TOC/TON and POC/PON at the front and adjacent stations suggested inputs of organic nitrogen while high TOC/TON in the northern and southern stations pointed to the removal of organic nitrogen (including PON), possibly through microbial regeneration and/or metazoan grazing (Table II) (Hansell and Waterhouse, 1997; Ogawa *et al.*, 1999).

Microbial loop dynamics in relation to hydrographic and biotic factors

High bacterial activity at the front is consistent with a heterotrophic community actively influencing carbon and nitrogen cycles and may involve complex interplay between hydrography of the frontal zone and top-down population controls of viral lysis and protist grazing pressure (Hagström *et al.*, 1988; Bratbak *et al.*, 1990). The observation of larger bacteria at the front could be explained by a higher abundance of bacterial phylotype(s) of a larger size (Morán and Calvo-Díaz, 2009; McCarren *et al.*, 2010). However, this observation could also be due to abundant viral particles within the cells and/or to rapid uptake and incorporation of labile viral lysate into the biomass (Parada *et al.*, 2006; Malits and Weinbauer, 2009). Virus:bacteria ratios were high in surface samples at the front and the oligotrophic station, but lower at the depth in the mesotrophic station and with depth in the front. Positive deviations from the canonical 10:1 ratio suggest enhanced viral-mediated bacterial mortality in the bulk seawater and/or at the micrometer scale (Seymour *et al.*, 2006; Suttle, 2007; Yang *et al.*, 2010).

Nano- and microflagellate abundance patterns also varied between the different water masses. Low abundance and high cell-specific BC observed at the front may reflect grazing by protists (Andersson *et al.*, 1986). Direct interception feeding by heterotrophic nanoflagellates is size-selective and can disproportionately remove larger bacteria (Monger and Landry, 1991, 1992). The high relative abundance of large bacteria at the front may therefore suggest a different balance between bacterial growth and removal processes. As noted above, A-Front was characterized by elevated organic matter, bacterial growth rates and bacterial biomass production. Low heterotrophic nanoflagellate abundance at the front is consistent with large, fast-growing bacterial cells within the front likely experiencing a low grazing impact. Compared with typical bacteria:nanoflagellate ratios of 1000:1 (Sanders *et al.*, 1992), higher ratios (~2000) at the surface of the front and at mesotrophic stations further support a reduced nanoflagellate grazing impact on bacteria (Fig. 3). As a major predator of nanoflagellates, microflagellates may have been responsible for maintaining reduced nanoflagellate abundance as our data show maximal heterotrophic nanoflagellate abundance coinciding with the lowest microflagellate abundance in mesotrophic waters (Supplementary data, Table S1). Greater mesozooplankton and copepod nauplii biomass at the front may have been an additional source of nanoflagellate mortality (Ohman *et al.*, 2012).

To compensate for the absence of grazing rate measurements and to test the above predictions, $\log_{10}$ transformed nanoflagellate abundance versus $\log_{10}$ transformed bacterial abundance was plotted and analyzed using the framework of maximum attainable abundance (MAA) and mean realized abundance (MRA) of nanoflagellates (Gasol, 1994) (Figs 4). Data points that lie near or above the MAA line suggest bottom-up control of nanoflagellate populations (in this case by bacterial prey) while points on or below the MRA line suggest top-down

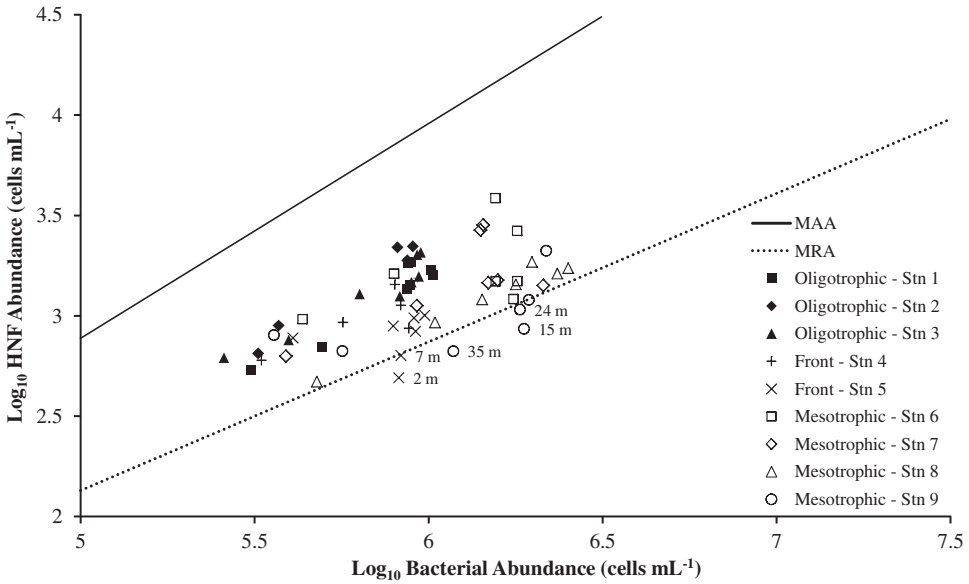

Fig. 4. $\log_{10}$ transformed heterotrophic nanoflagellate (HNF) versus $\log_{10}$ transformed bacterial abundance for all stations and depths. The solid line is the maximum attainable abundance (MAA) and the dotted line is the mean realized abundance (MRA).

forcing by nanoflagellate predators (such as microflagellates). Bottom-up control of nanoflagellates by bacterial availability was not significant. However, top-down control was apparent for the frontal and mesotrophic stations. While surface data for stations 6 and 7 were on the MRA line, stations 5 and 9 with depths of 2 and 7 m and 15, 24 and 35 m, respectively, were below the MRA line and thus likely exhibited significant predation of nanoflagellates. Collectively, these observations support the proposed mechanism at the front whereby increased grazing by microflagellates upon nanoflagellate bacteriovores led to a bacterial population comprised of fast-growing, larger cells predominantly regulated by viral lysis. Through viral lysis, bacterial cell abundance is decreased while the cell lysates could fuel elevated bacterial production through rapid and tightly coupled cycling of labile organic matter (Fuhrman, 1999).

Potential role of transparent particles

We considered the patterns of transparent particles and their capacity as microenvironments to identify their contribution to nutrient cycling and carbon export to the mesopelagic. The size and concentration profiles suggest potential roles of the microbial communities in particle formation and degradation. The maxima of TEP and FFP concentrations were not accompanied by average particle size maxima at any depth (Supplementary data, Fig. S5). This was unexpected, particularly at the front, where FFP concentrations were among the lowest measured while TEP concentration was elevated in comparison with the mesotrophic stations (Supplementary data, Fig. S5A and C). Interestingly, the depth at the front that exhibited maximal FFP average area and slightly elevated TEP average area also had the largest bacterial cell sizes (Supplementary data, Fig. S5B and D). We did not constrain the mechanisms underlying these observations, but they may include varied POM-colloid-DOM transformations involving viral, bacterial and abiotic processes.

Potential influences of frontal hydrodynamics on biogeochemistry in the CCE

The spatial stability of the A-Front was demonstrated by several transects with a moving vessel profiler that showed enhanced chl *a* concentrations and particulate biovolume at the frontal zone east of the transect (Ohman *et al.*, 2012) as well as satellite data depicting the frontal stability of the SST and chl *a* for 3 weeks prior to the transect (Kahru *et al.*, 2012). The eastward velocity along the frontal jet approached 0.3 m s^{-1} (Li *et al.*, 2012), and was thus capable of rapidly advecting plankton tens of kilometers within a few days. As a result, enhanced biological production along the frontal zone likely had biogeochemical consequences for adjacent regions within the CCE despite being spatially confined. The timescales of transport are also relevant for constraining and characterizing the growth responses of the microbial community and the formation and removal of non-living carbon (DOM, POM and transparent particles). Front-induced enhancement of the autochthonous biomass and particles was also evident in the higher photosynthetic potential of phytoplankton (Chekalyuk *et al.*, 2012) mediated by elevated diapycnal nitrate fluxes (Li *et al.*, 2012). If the present observations can be extrapolated to other frontal zones in the CCE, these features may be important environments where physically driven nutrient inputs upshift trophic interactions and biogeochemical cycling.

Formed at the interface of oligotrophic and mesotrophic water masses in the CCE, the A-Front was an enhanced microhabitat of high photosynthetic biomass, dynamic formation and removal of dissolved and particulate organic matter, elevated substrate processing and uptake activity by heterotrophic bacteria, and atypical relative abundances of viral, flagellate and zooplankton mortality agents. Although the scales of physical perturbations in the frontal zones are relatively small, such microbially mediated responses may, in the aggregate, affect carbon cycling and export processes on larger scales.

SUPPLEMENTARY DATA

Supplementary data can be found online at http://plankt.oxfordjournals.org.

ACKNOWLEDGEMENTS

We thank the participants of the CCE-LTER and the captain and the crew of the RV Melville. The questions, insights and suggestions of two anonymous reviewers also contributed significantly to the manuscript and the authors are very appreciative of their careful observations and feedback.

FUNDING

This work was supported by U.S. National Science Foundation grants OCE 04–17616 and 10-26607 for

the CCE-LTER Program; OCE-0548275 to L.I.A.; and by a grant from the Gordon and Betty Moore Foundation Marine Microbiology Initiative to F.A.

REFERENCES

Alldredge, A. L., Passow, U. and Logan, B. E. (1993) The abundance and significance of a class of large, transparent organic particles in the ocean. *Deep-Sea Res. I*, **40**, 1131–1140.

Aluwihare, L. I. and Repeta, D. J. (1999) A comparison of the chemical characteristics of oceanic DOM and extracellular DOM produced by marine algae. *Mar. Ecol. Prog. Ser.*, **186**, 105–117.

Andersson, A., Larsson, U. and Hagström, Å. (1986) Size-selective grazing by a microflagellate on pelagic bacteria. *Mar. Ecol. Prog Ser.*, **33**, 51–57.

Azam, F., Fenchel, T., Field, J. G. *et al.* (1983) The ecological role of water-column microbes in the sea. *Mar. Ecol. Prog. Ser.*, **10**, 257–263.

Azam, F. and Malfatti, F. (2007) Microbial structuring of marine ecosystems. *Nat. Rev. Microbiol.*, **5**, 782–791.

Bratbak, G. (1985) Bacterial biovolume and biomass estimations. *Appl. Environ. Microbiol.*, **49**, 1488–1493.

Bratbak, G., Heldal, M., Norland, S. *et al.* (1990) Viruses as partners in spring bloom microbial trophodynamics. *Appl. Environ. Microbiol.*, **56**, 1400–1405.

Bray, N. A., Keyes, A. and Morawitz, W. M. L. (1999) The california current system in the southern California bight and the Santa Barbara Channel. *J. Geophys. Res.*, **104**, 7695–7714.

Brussaard, C. P. D. (2004) Optimization of procedures for counting viruses by flow cytometry. *Appl. Environ. Microbiol.*, **70**, 1506–1513.

Chekalyuk, A., Landry, M. R., Goericke, R. *et al.* (2012) Laser fluorescence analysis of phytoplankton across a frontal zone in the California Current ecosystem. *J. Plank. Res.*, **34**, 761–777.

Cho, B. C. and Azam, F. (1988) Major role of bacteria in biogeochemical fluxes in the oceans interior. *Nature*, **332**, 441–443.

Claustre, H., Kerhervé, P., Marty, J. C. *et al.* (1994) Phytoplankton dynamics associated with a geostrophic front: ecological and biogeochemical implications. *J. Mar. Res.*, **52**, 711–742.

Cole, J. J., Findlay, S. and Pace, M. L. (1988) Bacterial production in fresh and saltwater ecosystems: a cross-system overview. *Mar. Ecol. Prog Ser.*, **43**, 1–10.

Del Giorgio, P. A. and Cole, J. J. (1998) Bacterial growth efficiency in natural aquatic systems. *Annu. Rev. Ecol. Syst.*, **29**, 503–541.

Ducklow, H. W. (2000) Bacterial production and biomass in the oceans. In Kirchman, D. L. (ed.), *Microbial Ecology of the Oceans*. 1st edn. Wiley-Blackwell, Hoboken, New Jersey, USA, pp. 85–120.

Ducklow, H. W. and Hill, S. M. (1985) Tritiated-thymidine incorporation and the growth of heterotrophic bacteria in warm core rings. *Limnol. Oceanogr.*, **30**, 260–272.

Ducklow, H. W., Smith, D. C., Campbell, L. *et al.* (2001) Heterotrophic bacterioplankton in the Arabian Sea: Basinwide response to year-round high primary productivity. *Deep-Sea Res. II*, **48**, 1303–1323.

Ewart, C. S., Meyers, M. K., Wallner, E. R. *et al.* (2008) Microbial dynamics in cyclonic and anticyclonic mode-water eddies in the northwestern Sargasso Sea. *Deep-Sea Res. II*, **55**, 1334–1347.

Falkowski, P. G., Ziemann, D., Kolber, Z. *et al.* (1991) Role of eddy pumping in enhancing primary production in the ocean. *Nature*, **352**, 55–58.

Fernández, M., Bianchi, M. and Vanwambeke, F. (1994) Bacterial biomass, heterotrophic production and utilization of dissolved organic matter photosynthetically produced in the Almeria-Oran front. *J. Mar. Syst.*, **5**, 313–325.

Fiala, M., Sournia, A., Claustre, H. *et al.* (1994) Gradients of phytoplankton abundance, composition and photosynthetic pigments across the Almeria-Oran front (SW Mediterranean Sea). *J. Mar. Syst.*, **5**, 223–233.

Franks, P. J. S. (1992) Sink or swim: accumulation of biomass at fronts. *Mar. Ecol. Prog. Ser.*, **82**, 1–12.

Fuhrman, J. A. (1999) Marine viruses and their biogeochemical and ecological effects. *Nature*, **399**, 541–548.

Fuhrman, J. A., Eppley, R. W., Hagstrom, A. *et al.* (1985) Diel variations in bacterioplankton, phytoplankton, and related parameters in the Southern California Bight. *Mar. Ecol. Prog. Ser.*, **27**, 9–20.

Gasol, J. M. (1994) A framework for the assessment of top-down vs bottom-up control of heterotrophic nanoflagellate abundance. *Mar. Ecol. Prog. Ser.*, **113**, 291–300.

Goericke, R. (2002) Top-down control of phytoplankton biomass and community structure in the monsoonal Arabian Sea. *Limnol. Oceanogr.*, **47**, 1307–1323.

Hagström, Å., Ammerman, J. W., Henrichs, S. *et al.* (1984) Bacterioplankton growth in seawater: 2. Organic matter utilization during steady-state growth in seawater cultures. *Mar. Ecol. Prog Ser.*, **18**, 41–48.

Hagström, Å., Azam, F., Andersson, A. *et al.* (1988) Microbial loop in an oligotrophic pelagic marine ecosystem: possible roles of cyanobacteria and nanoflagellates in the organic fluxes. *Mar. Ecol. Prog Ser.*, **49**, 171–178.

Hagström, Å., Larsson, U., H?rstedt, P. *et al.* (1979) Frequency of dividing cells, a new approach to the determination of bacterial growth rates in aquatic environments. *Appl. Environ. Microbiol.*, **37**, 805–812.

Hansell, D. A. and Waterhouse, T. Y. (1997) Controls on the distributions of organic carbon and nitrogen in the eastern Pacific Ocean. *Deep-Sea Res. I*, **44**, 843–857.

Heinänen, A., Kononen, K., Kuosa, H. *et al.* (1995) Bacterioplankton growth associated with physical fronts during a cyanobacterial bloom. *Mar. Ecol. Prog Ser.*, **116**, 233–245.

Hoppe, H. G., Gocke, K., Koppe, R. *et al.* (2002) Bacterial growth and primary production along a north-south transect of the Atlantic Ocean. *Nature*, **416**, 168–171.

Kähler, P. and Koeve, W. (2001) Marine dissolved organic matter: can its C : N ratio explain carbon overconsumption? *Deep-Sea Res. I*, **48**, 49–62.

Kahru, M., Di Lorenzo, E., Manzano-Sarabia, M. *et al.* (2012) Spatial and temporal statistics of surface temperature and chlorophyll fronts in the California Current. *J. Plank. Res.*, **34**, 749–760.

Karl, D. M., Hebel, D. V., Bjorkman, K. *et al.* (1998) The role of dissolved organic matter release in the productivity of the oligotrophic North Pacific Ocean. *Limnol. Oceanogr.*, **43**, 1270–1286.

Kirchman, D., K'nees, E. and Hodson, R. (1985) Leucine incorporation and its potential as a measure of protein synthesis by bacteria in natural aquatic systems. *Appl. Environ. Microbiol.*, **49**, 599–607.

Kirchman, D. L., Suzuki, Y., Garside, C. *et al.* (1991) High turnover rates of dissolved organic carbon during a spring phytoplankton bloom. *Nature*, **352**, 612–614.

Landry, M. R., Ohman, M. D., Goericke, R. *et al.* (2012) Pelagic community responses to a deep-water front in the California Current Ecosystem: overview of the A-Front Study. *J. Plank. Res.*, **34**, 739–748.

Li, Q. P., Franks, P. J. S., Ohman, M. D. *et al.* (2012) Enhanced nitrate fluxes and biological processes at a frontal zone in the Southern California Current System. *J. Plank. Res.*, **34**, 790–801.

Libby, P. S. and Wheeler, P. A. (1997) Particulate and dissolved organic nitrogen in the central and eastern equatorial Pacific. *Deep-Sea Res. I*, **44**, 345–361.

Mague, T. H., Friberg, E., Hughes, D. J. *et al.* (1980) Extracellular release of carbon by marine phytoplankton; a physiological approach. *Limnol. Oceanogr.*, **25**, 262–279.

Malfatti, F., Samo, T. J. and Azam, F. (2010) High-resolution imaging of pelagic bacteria by Atomic Force Microscopy and implications for carbon cycling. *ISME J.*, **4**, 427–439.

Malits, A. and Weinbauer, M. G. (2009) Effect of turbulence and viruses on prokaryotic cell size, production and diversity. *Aquat. Microb. Ecol.*, **54**, 243–254.

Martin, J. H., Coale, K. H., Johnson, K. S. *et al.* (1994) Testing the iron hypothesis in ecosystems of the equatorial Pacific Ocean. *Nature*, **371**, 123–129.

Mccarren, J., Becker, J. W., Repeta, D. J. *et al.* (2010) Microbial community transcriptomes reveal microbes and metabolic pathways associated with dissolved organic matter turnover in the sea. *Proc. Natl. Acad. Sci. U. S. A.*, **107**, 16420–16427.

Monger, B. C. and Landry, M. R. (1991) Prey-size dependency of grazing by free-living marine flagellates. *Mar. Ecol. Prog. Ser.*, **74**, 239–248.

Monger, B. C. and Landry, M. R. (1992) Size-selective grazing by heterotrophic nanoflagellates: an analysis using live-stained bacteria and dual-beam flow cytometry. *Adv. Limnol.*, **37**, 173–185.

Monger, B. C. and Landry, M. R. (1993) Flow cytometric analysis of marine bacteria with Hoechst 33342. *Appl. Environ. Microbiol.*, **59**, 905–911.

Morán, X. A. G. and Calvo-Díaz, A. (2009) Single-cell vs. bulk activity properties of coastal bacterioplankton over an annual cycle in a temperate ecosystem. *FEMS Microbiol. Ecol.*, **67**, 43–56.

Morán, X. A. G., Taupier-Letage, I., Vázquez-Domínguez, E. *et al.* (2001) Physical-biological coupling in the Algerian Basin (SW Mediterranean): influence of mesoscale instabilities on the biomass and production of phytoplankton and bacterioplankton. *Deep-Sea Res. I*, **48**, 405–437.

Ogawa, H., Fukuda, R. and Koike, I. (1999) Vertical distributions of dissolved organic carbon and nitrogen in the Southern Ocean. *Deep-Sea Res. I*, **46**, 1809–1826.

Ogawa, H. and Tanoue, E. (2003) Dissolved organic matter in oceanic waters. *J. Oceanogr.*, **59**, 129–147.

Ohman, M. D., Powell, J., Picheral, M. *et al.* (2012) Mesozooplankton and particulate matter responses to a deep-water frontal system in the southern California Current System. *J. Plank. Res.*, **34**, 815–827.

Pallàs-Sanz, E., Johnston, T. M. S. and Rudnick, D. L. (2010) Frontal dynamics in a California Current system shallow front: 1. Frontal processes and tracer structure. *J. Geophys. Res.*, **115**, 14.

Parada, V., Herndl, G. J. and Weinbauer, M. G. (2006) Viral burst size of heterotrophic prokaryotes in aquatic systems. *J. Mar. Biol. Assoc. U.K.*, **86**, 613–621.

Patel, A., Noble, R. T., Steele, J. A. *et al.* (2007) Virus and prokaryote enumeration from planktonic aquatic environments by epifluorescence microscopy with SYBR Green I. *Nat. Protoc.*, **2**, 269–276.

Peinert, R. and Miquel, J. C. (1994) The significance of frontal processes for vertical particle fluxes: a case study in the Alboran Sea (SW Mediterranean Sea). *J. Mar. Syst.*, **5**, 377–389.

Prieur, L. and Sournia, A. (1994) Almofront-1 (April-May 1991): an interdisciplinary study of the Almeria-Oran geostrophic front, SW Mediterranean Sea. *J. Mar. Syst.*, **5**, 187–203.

Raven, J. A. and Falkowski, P. G. (1999) Oceanic sinks for atmospheric CO_2. *Plant Cell Environ.*, **22**, 741–755.

Redfield, A. C., Ketchum, B. H. and Richards, F. A. (1963) The influence of organisms on the composition of seawater. In Hill, M. N. (ed.), *The Sea.* Vol. 2. Wiley, New York, pp. 26–77.

Riemann, L., Nielsen, T. G., Kragh, T. *et al.* (2011) Distribution and production of plankton communities in the subtropical convergence zone of the Sargasso Sea. I. Phytoplankton and bacterioplankton. *Mar. Ecol. Prog. Ser.*, **426**, 57–70.

Rykaczewski, R. R. and Checkley, D. M. (2008) Influence of ocean winds on the pelagic ecosystem in, upwelling regions. *Proc. Natl. Acad. Sci. U. S. A.*, **105**, 1965–1970.

Samo, T. J., Malfatti, F. and Azam, F. (2008) A new class of transparent organic particles in seawater visualized by a novel fluorescence approach. *Aquat. Microb. Ecol.*, **53**, 307–321.

Sanders, R. W., Caron, D. A. and Berninger, U. G. (1992) Relationships between bacteria and heterotrophic nanoplankton in marine and fresh waters: an inter-ecosystem comparison. *Mar. Ecol. Prog. Ser.*, **86**, 1–14.

Schlitzer, R. (2008) Ocean Data View, version 4.5.0. http://odv.awi.de/.

Sempéré, R., Dafner, E., Van Wambeke, F. *et al.* (2003) Distribution and cycling of total organic carbon across the Almeria-Oran Front in the Mediterranean Sea: Implications for carbon cycling in the western basin. *J. Geophys. Res.*, **108**, 11.

Seymour, J. R., Seuront, L., Doubell, M. *et al.* (2006) Microscale patchiness of virioplankton. *J. Mar. Biol. Assoc. U.K.*, **86**, 551–561.

Simon, M., Alldredge, A. L. and Azam, F. (1990) Bacterial carbon dynamics on marine snow. *Mar. Ecol. Prog. Ser.*, **65**, 205–211.

Simon, M. and Azam, F. (1989) Protein content and protein synthesis rates of planktonic marine bacteria. *Mar. Ecol. Prog. Ser.*, **51**, 201–213.

Smith, D. C. and Azam, F. (1992) A simple, economical method for measuring bacterial protein synthesis rates in seawater using 3H-leucine. *Mar. Microb. Food Webs*, **6**, 107–114.

Suttle, C. A. (2007) Marine viruses: major players in the global ecosystem. *Nat. Rev. Microbiol.*, **5**, 801–812.

Taylor, A. G., Goericke, R., Landry, M. R. *et al.* (2012) Sharp gradients in phytoplankton community structure across a frontal zone in the California Current Ecosystem. *J. Plank. Res.*, **34**, 778–789.

Thingstad, T. F., Hagstrom, A. and Rassoulzadegan, F. (1997) Accumulation of degradable DOC in surface waters: is it caused by a malfunctioning microbial loop? *Limnol. Oceanogr.*, **42**, 398–404.

Van Wambeke, F., Lefèvre, D., Prieur, L. *et al.* (2004) Distribution of microbial biomass, production, respiration, dissolved organic

carbon and factors controlling bacterial production across a geostrophic front (Almeria-Oran, SW Mediterranean Sea). *Mar. Ecol.-Prog. Ser.*, **269**, 1–15.

Videau, C., Sournia, A., Prieur, L. *et al.* (1994) Phytoplankton and primary production characteristics at selected sites in the geostrophic Almeria-Oran front system (SW Mediterranean Sea). *J. Mar. Syst.*, **5**, 235–250.

Yang, Y. H., Motegi, C., Yokokawa, T. *et al.* (2010) Large-scale distribution patterns of virioplankton in the upper ocean. *Aquat. Microb. Ecol.*, **60**, 233–246.